

Generating Symmetry-Protected Long-Range Entanglement in Many-Body Systems

Shovan Dutta,^{1,2} Stefan Kuhr,³ and Nigel R. Cooper^{1,4}

¹*T.C.M. Group, Cavendish Laboratory, University of Cambridge, JJ Thomson Avenue, Cambridge CB3 0HE, United Kingdom*

²*Max Planck Institute for the Physics of Complex Systems, 01187 Dresden, Germany*

³*Department of Physics, University of Strathclyde, Glasgow G4 0NG, United Kingdom*

⁴*Department of Physics and Astronomy, University of Florence, Via G. Sansone 1, 50019 Sesto Fiorentino, Italy*

(Dated: January 27, 2022)

Entanglement between spatially distant qubits is perhaps the most counterintuitive and vital resource for distributed quantum computing [1, 2]. However, despite a few special cases [3–7], there is no known general procedure to maximally entangle two distant parts of an interacting many-body system. Here we present a symmetry-based approach, whereby one applies several timed pulses to drive a system to a particular symmetry sector with maximal bipartite long-range entanglement. As a concrete example, we demonstrate how a simple sequence of on-site pulses on a qubit array can efficiently produce any given number of stable nonlocal Bell pairs, realizable in several present-day atomic and photonic experimental platforms. More generally, our approach paves a route for novel state preparation by harnessing symmetry. For instance, we show how it enables the creation of long-sought-after superconducting η pairs [8–10] in a repulsive Hubbard model.

Since the early days of quantum mechanics, entanglement has been seen as a fundamental quantum trait, which now lies at the heart of quantum information processing [1, 2]. In recent decades, experiments have made great progress in generating entanglement between two isolated qubits via photon exchange [11–13] and combining such two-qubit gates to build multi-qubit states [14–16]. However, it is much harder to entangle a pair of distant qubits in a truly many-body environment where multiple qubits interact with one another [17]. Theoretical protocols have largely focused on creating a single Bell pair between two ends of a spin chain [18–21]. Although more pairs can be entangled using specially designed nonuniform coupling [3, 4] or correlated dissipation [5], these are seldom realized in experiments [22] and limited to free-fermionic chains.

Here, we introduce a general approach that leverages the existence of a symmetry to create entanglement over increasingly longer distances. Symmetry plays a fundamental role in modern physics [23]. As in classical mechanics, a symmetry in a quantum system is intimately linked to a conservation law, which divides the space of all states into decoupled sectors. We envision scenarios where these sectors can be characterized by increasing long-range entanglement, as in the examples below. Our idea is sketched in Fig. 1(a): Suppose the system is ini-

tially in some low-entangled state in sector \mathcal{S}_0 , e.g., the ground state or a product state. We apply a series of symmetry-breaking pulses to drive the system toward the maximally-entangled sector \mathcal{S}_* , hosting one or few states. The pulses are timed optimally to maximize this one-way transfer. If the transfer fidelity is high, one can produce a macroscopic weight in \mathcal{S}_* with a small number of pulses.

We will show how this technique allows one to generate Bell pairs between any number of mirror-conjugate sites in a uniform spin chain [Fig. 1(b)], realizing variants of the so-called “rainbow” states [24, 25]. These states possess a high persistency of entanglement [26] and can be used to efficiently distribute entanglement in a quantum network [3]. Unlike other protocols for creating rainbow-like states, we do not require the spin-spin interactions to be selectively switched off [14], individually fine tuned [3, 4, 22, 24], or coupled with engineered dissipation for slow relaxation [5, 6]. Instead, our scheme uses only local π pulses that are standard in experiments. The Bell pairs are created in a time linear in system size, and stable thereafter due to the symmetry conservation.

Crucially, our approach extends beyond spin chains to arbitrary interacting systems with a similar symmetry structure. In particular, we will show how one can drive a Fermi-Hubbard chain [27] toward an elusive maximally-correlated η -pairing state [8]. Further, since our protocol is symmetry based, the entanglement generated is robust against any perturbations that preserve the symmetry.

Qubit-array protocol.—We consider the simplest spin-1/2 XX Hamiltonian with $2l + 1$ sites for integer l ,

$$\hat{H} = -(J/4) \sum_{i=-l}^{l-1} \hat{\sigma}_i^x \hat{\sigma}_{i+1}^x + \hat{\sigma}_i^y \hat{\sigma}_{i+1}^y, \quad (1)$$

where the $\hat{\sigma}$'s are the Pauli spin operators and J is the spin-spin coupling ($\hbar = 1$). This model can be reduced to free fermions through a Jordan-Wigner (JW) map, $\hat{f}_i = \hat{\sigma}_i^- \prod_{j<i} \hat{\sigma}_j^z$, where $\hat{\sigma}_i^\pm := (\hat{\sigma}_i^x \pm i\hat{\sigma}_i^y)/2$ and \hat{f}_i^\dagger creates a fermion at site i , yielding $\hat{H} = -(J/2) \sum_i \hat{f}_i^\dagger \hat{f}_{i+1} + \text{h.c.}$. Thus, spins \uparrow and \downarrow correspond to filled and empty sites, respectively, in the fermion picture, and the occupation of each fermionic single-particle mode is conserved.

In particular, as shown in Ref. [6], there is a crucial symmetry relating to the entanglement between left and right halves of the chain, given by the symmetry operator

$$\hat{C} = \hat{\sigma}_0^z/2 + \sum_{i=1}^l (\hat{f}_i^\dagger \hat{f}_{-i} + \text{h.c.}). \quad (2)$$

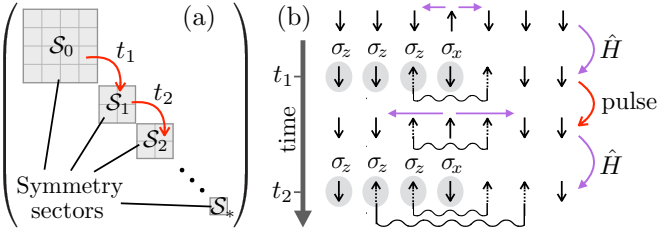


FIG. 1. **Sketch of the protocol and its application to a qubit array.** (a) Schematic of how one can sequentially transfer a many-body system through symmetry sectors S_n to prepare a maximally-entangled state in S_k by a sequence of pulses at optimal times t_n . The block-diagonal structure represents the undriven Hamiltonian \hat{H} . (b) Illustration for a symmetric spin-1/2 chain: π pulses create \uparrow spins at the center site, which then spread under the Hamiltonian, giving rise to multiple Bell pairs between mirror-conjugate sites.

Here, $\hat{\sigma}_0^z$ measures the fermion-number parity at the center site, and the terms $\hat{f}_i^\dagger \hat{f}_{-i}$ exchange spins between mirror-conjugate sites i and $-i$ with a phase given by the total parity in between. The nature of this exchange becomes clearer if one rewrites Eq. (2) as $\hat{C} = \hat{\sigma}_0^z/2 + \sum_{i=1}^l \hat{a}_{i,+}^\dagger \hat{a}_{i,+} - \hat{a}_{i,-}^\dagger \hat{a}_{i,-}$, where $\hat{a}_{i,\pm} := (\hat{f}_i \pm \hat{f}_{-i})/\sqrt{2}$. Here, $\hat{a}_{i,\pm}^\dagger$ creates a Bell pair between sites i and $-i$, $\hat{a}_{i,\pm}^\dagger |\text{vac}\rangle \propto |\uparrow_i \downarrow_{-i}\rangle \pm |\downarrow_i \uparrow_{-i}\rangle$, where $|\text{vac}\rangle$ is the vacuum state with all spins \downarrow . The symmetric and antisymmetric Bell pairs can be thought of as having a “charge” of ± 1 , such that \hat{C} measures the net “charge” of all such pairs. Conversely, this “charge” quantum number is 0 for the states $|\downarrow_i \downarrow_{-i}\rangle$ and $|\uparrow_i \uparrow_{-i}\rangle = \hat{a}_{i,+}^\dagger \hat{a}_{i,-}^\dagger |\text{vac}\rangle$, so it counts the number of Bell pairs at $\{i, -i\}$ up to a sign. Therefore, the eigenvalues of \hat{C} vary from $\lambda = -l - 1/2$ to $\lambda = l + 1/2$ in steps of 1, where the $\pm 1/2$ arises from $\hat{\sigma}_0^z/2$. In each of the sectors $\lambda = \pm(l + 1/2)$, there is a single state that is maximally entangled with a Bell pair at all positions, given by $|\Psi_\pm\rangle \propto |\pm\rangle_0 \prod_{i=1}^l (|\uparrow_i \downarrow_{-i}\rangle + (-1)^i |\downarrow_i \uparrow_{-i}\rangle)$, where $|+\rangle \equiv |\uparrow\rangle$, $|-\rangle \equiv |\downarrow\rangle$, and the alternating phase $(-1)^i$ originates from the JW string. Smaller absolute values of λ correspond to states with fewer Bell pairs on average, and all product states have $\langle \hat{C} \rangle = \pm 1/2$.

Our strategy is to start from the vacuum state with $\lambda = -1/2$ and apply a sequence of timed pulses to reach the state $|\Psi_+\rangle$. For this, one can increase λ by 1 by flipping the center spin from \downarrow to \uparrow [see Eq. (2)]. However, one has to ensure it does not affect the exchange terms $\hat{f}_i^\dagger \hat{f}_{-i}$ which also depend on the center spin. Thus, instead of a π pulse at the center site alone, one has to apply a fermionic pulse, e.g., $\hat{f}_0 + \hat{f}_0^\dagger = \hat{\sigma}_0^x \prod_{i<0} \hat{\sigma}_i^z$, which commutes with $\hat{f}_i^\dagger \hat{f}_{-i} \forall i \neq 0$. This amounts to applying simultaneous local π pulses on half the qubits, which can be readily implemented in experiments. Under such a fermionic pulse, $\langle \hat{C} \rangle \rightarrow \langle \hat{C} \rangle - \langle \hat{\sigma}_0^z \rangle$, so if the center spin is \downarrow when the pulse is applied, $\langle \hat{C} \rangle$ increases by 1.

Figure 1(b) shows the resulting protocol: Flipping the center spin of the vacuum state gives $\lambda = 1/2$ and pro-

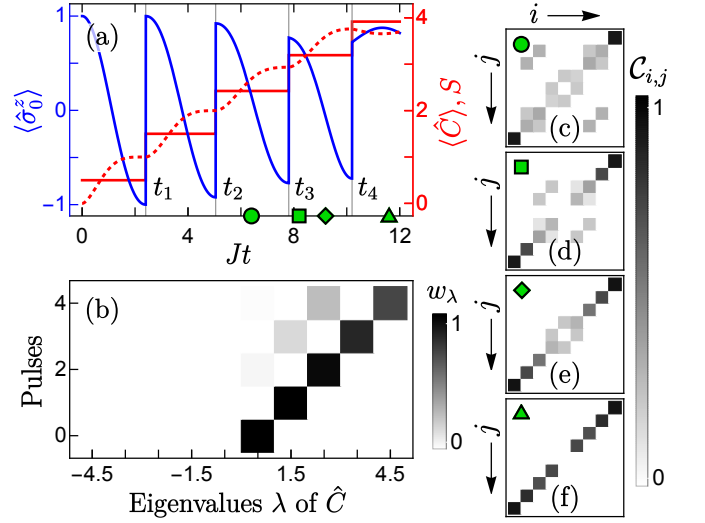


FIG. 2. **Generation of multiple nonlocal Bell pairs.** (a) Time evolution of the center-spin magnetization $\langle \hat{\sigma}_0^z \rangle$ of a 9-site spin-1/2 XX chain using exact diagonalization. The center spin is flipped whenever $\langle \hat{\sigma}_0^z \rangle$ reaches a minimum below 0, which increases the expectation of the symmetry \hat{C} (horizontal lines) that relates to the number of Bell pairs between mirror-conjugate sites. Accordingly, the von Neumann entropy S between two sides of the chain grows monotonically (dotted curve). (b) Weights w_λ in different symmetry sectors after each pulse, showing a high-fidelity transfer toward more strongly-entangled states. (c-f) Pairwise concurrence $C_{i,j}$ between sites i and j (with $C_{i,i} \equiv 0$) at times indicated by the green labels in (a), showing how the Bell pairs at $\{i, -i\}$ are successively stacked inward until all positions are filled.

duces a spin- \uparrow impurity that spreads out in both directions [28], entangling those sites. During this spreading, λ is unaltered as $[\hat{H}, \hat{C}] = 0$. After a time $t_1 \sim 2/J$, the center site points \downarrow again, when we apply the next pulse, producing another \uparrow spin and increasing λ by 1. Repeating this process l times gets one to the state $|\Psi_+\rangle$ with l Bell pairs in a time $t_l \sim 2l/J$.

The protocol is not perfect as the center does not fully relax to a spin- \downarrow state after the second pulse, as shown in Fig. 2(a), where we apply the following pulses whenever $\langle \hat{\sigma}_0^z \rangle$ is minimum (and negative) for the first time. Due to the spin- \uparrow component, there is a small likelihood that λ decreases by 1 during the spin flip. However, as shown in Fig. 2(b), the distribution remains strongly peaked at the target sector $\lambda = n + 1/2$ after the n -th pulse. As a result, both $\langle \hat{C} \rangle$ and the entanglement entropy between left and right halves are near maximal at the end of the sequence [see Fig. 2(a)]. Furthermore, the entanglement is distilled in the form of Bell pairs, which is unusual even for highly-entangled states [17]. Such Bell pairs between mirror-conjugate sites are seen in Fig. 2(f) where we plot the concurrence between sites i and j , which is a robust measure of entanglement between two qubits [29] that increases from 0 when the qubits are not entangled to 1

when they are maximally entangled.

Figure 2(c) shows the first of these Bell pairs is established between the two end sites when the first \uparrow spin arrives at $t \sim l/J$. Each subsequent pulse adds one more Bell pair toward the center [Figs. 2(d-f)]. This stacking is also evident in the experimentally measurable spin-spin correlations (see Extended Data Fig. 1).

Finite-size scaling.—As l is increased, the fidelity decreases gradually and saturates for $l \gtrsim 10$, where $\langle \hat{C} \rangle \approx 0.6l + 1$ after the pulse sequence (Extended Data Fig. 2), i.e., the number of generated Bell pairs grows linearly with the number of qubits, as does the preparation time $t \sim 2l/J$. This scaling is on par with more complex protocols using two-qubit gates [14] or nonuniform coupling [3, 4], and much faster than using correlated dissipation [5, 6]. The fidelity can be enhanced further by optimal pulse shaping [30, 31]. Moreover, one can project the final state exactly onto $|\Psi_+\rangle$ by measuring the spin imbalance $\hat{\sigma}^z := \sum_i \hat{\sigma}_i^z$, which is locked to \hat{C} as $\hat{\sigma}^z = 2(\hat{C} - l)$, since λ is changed by flipping a spin.

Robustness.—Figure 3 shows the protocol is relatively insensitive to many generic imperfections found in experiments. In particular, the fidelity $\langle \hat{C} \rangle$ is affected only to second order in common Hamiltonian perturbations (see Methods). This includes both symmetry-preserving cases, such as an x - y anisotropy, and symmetry-breaking perturbations, such as a z - z coupling, random Zeeman splittings, or next-nearest-neighbor coupling.

If a perturbation commutes with both \hat{C} and $\hat{\sigma}_0^z$, the full time evolution of $\langle \hat{C} \rangle$ is unaltered, as in the case of a uniform magnetic field along z . For other symmetry-preserving perturbations, including reflection-symmetric potentials [6] and dephasing at the center site, the fidelity may be affected but the generated entanglement is stable. If the symmetry itself is broken, $\langle \hat{C} \rangle$ attains a maximum value *during* the protocol.

Experimental realization.—The protocol can be implemented on several experimental platforms that have the capability of single-site addressing, particularly quantum-gas microscopes [32], superconducting circuits [33], and arrays of Rydberg atoms [34].

Quantum-gas microscope experiments allow us to flip the spin of individual atoms in a chain with high accuracy using a tightly focused laser beam and a microwave field [28]. Using two-component bosons at unit filling in the limit of strong interactions realizes a Heisenberg chain through virtual spin exchange [35]. By separately tuning the intra- and inter-species interactions, one can set the z - z coupling to 0, producing the XX model [36].

The XX spin-1/2 chain has also been realized using capacitively coupled transmon qubits in a superconducting circuit [37], where one can perform arbitrary single-qubit rotations [33]. The dominant errors come from on-site dephasing and disorder, which are both hundreds of times smaller than J in present-day setups [37].

Resonant dipole-dipole interactions between Rydberg

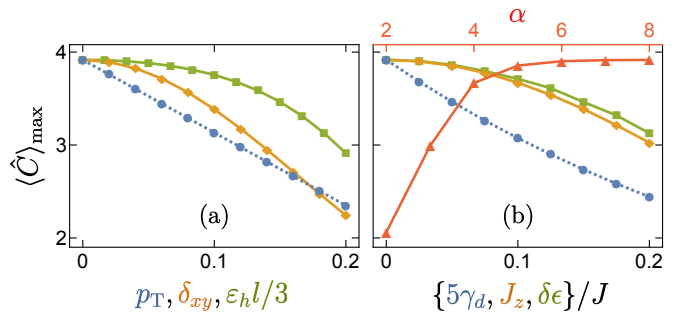


FIG. 3. **Robustness to generic imperfections.** Fidelity, measured by the maximum value of $\langle \hat{C} \rangle$ attained, for 9 sites in the presence of (a) symmetry-preserving and (b) symmetry-breaking, unitary (solid) and non-unitary (dotted) perturbations: (a) p_T is a defect probability of starting with an \uparrow spin at any given site; δ_{xy} is the anisotropy for an XY chain, $\delta_{xy} := (J_x - J_y)/(J_x + J_y)$; ε_h is a harmonic-trap-induced inhomogeneity, such that $J_{i,i+1} = J/[1 - \varepsilon_h^2(i + 1/2)^2]$ [28]; (b) γ_d is a uniform dephasing rate, modeled by Lindblad operators $\sqrt{\gamma_d}\hat{\sigma}_i^z/2$ (see Methods); J_z is the z - z coupling for an XXZ chain; $\delta\epsilon$ is a disorder strength that gives $\hat{H}' = \sum_i \epsilon_i \hat{\sigma}_i^z$ where ϵ_i are randomly distributed in $[-\delta\epsilon/2, \delta\epsilon/2]$; α characterizes long-range interactions $J_{i,j} = J/|i-j|^\alpha$. For disorder, dephasing, and thermal defects, $\langle \hat{C} \rangle$ is ensemble averaged.

excitations in a chain of atoms also yields an XX model but with long-range coupling, $J_{i,j} = J/|i-j|^\alpha$ with $\alpha = 3$ [34], which breaks the symmetry \hat{C} . Nonetheless, one can obtain fidelities of up to 75% for 9 sites [Fig. 3(b)]. For trapped-ion chains [38], however, α is typically limited to smaller values, making the protocol less viable.

Generalizations: η pairing.—Having demonstrated our approach for a free-fermionic spin chain, we now consider a genuinely interacting system, namely the celebrated Fermi-Hubbard model [27] with $2l$ sites,

$$\hat{H} = \sum_{s=\uparrow,\downarrow} \sum_{i=-l}^{l-1} (-J \hat{c}_{i,s}^\dagger \hat{c}_{i+1,s} + \text{h.c.}) + U \sum_{i=-l}^l \hat{n}_{i,\uparrow} \hat{n}_{i,\downarrow}. \quad (3)$$

Here, $\hat{c}_{i,s}^\dagger$ creates a fermion with spin s at site i , $\hat{n}_{i,s} := \hat{c}_{i,s}^\dagger \hat{c}_{i,s}$ gives the site occupation, J is now the nearest-neighbor tunneling, and $U > 0$ is an on-site repulsion. It has been known since the 90s that \hat{H} has eigenstates with long-range superconducting order [8], thanks to an SU(2) symmetry with generators $\hat{\eta}^- = \sum_i (-1)^i \hat{c}_{i,\uparrow} \hat{c}_{i,\downarrow}$, $\hat{\eta}^+ = \hat{\eta}^{-\dagger}$, and $\hat{\eta}^z = \sum_i (\hat{n}_{i,\uparrow} + \hat{n}_{i,\downarrow} - 1)/2$. Here, $\hat{\eta}^+$ acting on the vacuum $|0\rangle$ creates a bound pair (doublon) with quasimomentum π (an η pair), which leads to staggered superconducting pair correlations $P_{i,j} = \langle \hat{c}_{i,\downarrow}^\dagger \hat{c}_{i,\uparrow}^\dagger \hat{c}_{j,\uparrow} \hat{c}_{j,\downarrow} \rangle$. In particular, at half filling ($\hat{\eta}^z = 0$), the correlations are maximal for an η condensate $|Y\rangle \propto (\hat{\eta}^+)^l |0\rangle$, which gives $P_{i,j} = (-1)^{i+j} l / (4l - 2) \forall i \neq j$ [8]. However, producing an η pair costs energy U , so $|Y\rangle$ is a highly-excited state that is difficult to engineer in theory [10, 39–41] and has not been realized experimentally.

To prepare $|Y\rangle$ using pulses, we note that the num-

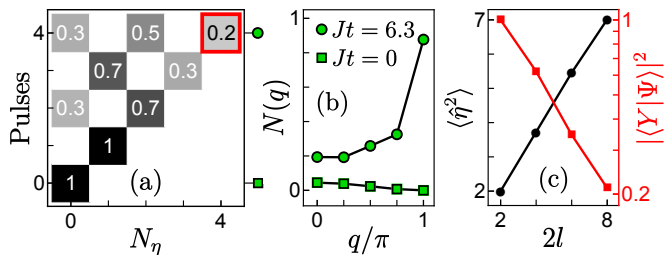


FIG. 4. **Generation of superconducting η pairs.** Evolution of a repulsive Fermi-Hubbard chain ($U/J = 10$), starting from an antiferromagnetic ground state at half filling, using exact diagonalization. (a) Distribution among symmetry sectors of $\hat{\eta}^2$ with different numbers of η pairs, N_η , after successive pulses for $2l = 8$ sites. The red square highlights a notable overlap with the maximally-correlated η condensate $|Y\rangle$. (b) Initial and final pair-momentum distributions, showing the emergence of a peak at the band edge, characteristic of η pairing. (c) The final value of $\langle \hat{\eta}^2 \rangle$ grows linearly with l , but the many-body overlap with $|Y\rangle$ falls exponentially [39].

ber of η pairs, N_η , is measured by the symmetry $\hat{\eta}^2 = \hat{\eta}^+ \hat{\eta}^- - \hat{\eta}^z + (\hat{\eta}^z)^2$ with eigenvalues $N_\eta(N_\eta + 1)$, where $N_\eta = 0, 1, \dots, l$ at half filling. The maximally-correlated $|Y\rangle$ is the only state having $N_\eta = l$. Further, as shown in Ref. [10], one can change N_η by ± 1 by applying the current operator $\hat{\mathcal{J}} = i \sum_{i,s} \hat{c}_{i+1,s}^\dagger \hat{c}_{i,s} + \text{h.c.}$: This amounts to changing $J \rightarrow iJ'(t)$ in Eq. (3) for a short pulse, which would be challenging to implement, but possible via laser-assisted tunneling [42] or lattice shaking [43].

Thus, we arrive at a conceptually simple protocol: Starting from an antiferromagnetic ground state with $N_\eta = 0$ for $U \gg J$, as realized in Ref. [44], we repeatedly apply $\hat{\mathcal{J}}$ when it would increase $\langle \hat{\eta}^2 \rangle$ the most. To this end, we monitor $\mathcal{T} := \langle \hat{\mathcal{J}} \hat{\eta}^2 \hat{\mathcal{J}} \rangle / \langle \hat{\mathcal{J}}^2 \rangle$ and apply the next pulse whenever \mathcal{T} is maximum over a virtual-tunneling time $\Delta t = U/(2J^2)$, the slowest time scale in the problem (see Extended Data Fig. 3). Figure 4(a) shows the state after l pulses has a significant overlap with $|Y\rangle$, which is reached in a time $t \sim 6/J$ for 8 sites, orders of magnitude faster than adiabatic [39] or dissipative [41] approaches. The η pairing is manifest in the pair-momentum distribution $N(q) = (2l)^{-1} \sum_{i,j} e^{iq(i-j)} P_{i,j}$ as a sharp peak at $q = \pi$ [Fig. 4(b)], which can be detected experimentally [45]. We find the preparation time and the final value of $\langle \hat{\eta}^2 \rangle$ both grow linearly with l [Fig. 4(c)], so the average number of η pairs grows as \sqrt{l} .

The Hubbard model also has a spin-SU(2) symmetry whose generators \hat{S}^\pm and \hat{S}^z are related to the η generators by a particle-hole transformation $c_{i,\downarrow} \rightarrow (-1)^{j+1} \hat{c}_{i,\downarrow}^\dagger$ [27]. Hence, there is a dual protocol for maximizing the total spin $\langle \hat{S}^2 \rangle$ for long-range spin-spin correlations, with the pulse operator $\hat{\mathcal{J}}_s = i \sum_i \hat{c}_{i+1,\uparrow}^\dagger \hat{c}_{i,\uparrow} - \hat{c}_{i+1,\downarrow}^\dagger \hat{c}_{i,\downarrow} + \text{h.c.}$, i.e., a spin-dependent complex tunneling as in Ref. [46].

Conclusions.—We have introduced a general technique for harnessing symmetries to produce on-demand long-

range entanglement in many-body quantum systems. The approach relies solely on the symmetry structure and can be readily extended to dissipative systems [6, 47, 48] and higher dimensions [8, 9]. For simplicity, we have assumed instantaneous pulses; one can obtain even higher fidelities by allowing more general waveforms using optimal control strategies [30, 31]. Together with advances in engineering many-body Hamiltonians [32–34, 38, 49] and dissipation [50], our technique paves an exciting route to synthesizing strongly-entangled quantum states with key applications to quantum information processing.

We thank Leonardo Bianchi and Berislav Buča for discussions. This work was supported by EPSRC Grant No. EP/P009565/1 and by a Simons Investigator Award.

-
- [1] R. Horodecki, P. Horodecki, M. Horodecki, and K. Horodecki, Quantum entanglement, *Rev. Mod. Phys.* **81**, 865 (2009).
 - [2] S. Wehner, D. Elkouss, and R. Hanson, Quantum internet: A vision for the road ahead, *Science* **362**, 303 (2018).
 - [3] C. Di Franco, M. Paternostro, and M. S. Kim, Nested entangled states for distributed quantum channels, *Phys. Rev. A* **77**, 020303 (2008).
 - [4] B. Alkurtass, L. Bianchi, and S. Bose, Optimal quench for distance-independent entanglement and maximal block entropy, *Phys. Rev. A* **90**, 042304 (2014).
 - [5] A. Pocklington, Y.-X. Wang, Y. Yanay, and A. A. Clerk, Stabilizing volume-law entangled states of fermions and qubits using local dissipation, [arXiv:2107.14121](https://arxiv.org/abs/2107.14121) (2021).
 - [6] S. Dutta and N. R. Cooper, Long-range coherence and multiple steady states in a lossy qubit array, *Phys. Rev. Lett.* **125**, 240404 (2020).
 - [7] A. I. Lotkov, V. Gritsev, A. K. Fedorov, and D. V. Kurlov, Floquet integrability and long-range entanglement generation in the one-dimensional quantum Potts model, [arXiv:2110.09559](https://arxiv.org/abs/2110.09559) (2021).
 - [8] C. N. Yang, η pairing and off-diagonal long-range order in a Hubbard model, *Phys. Rev. Lett.* **63**, 2144 (1989).
 - [9] S. Moudgalya, N. Regnault, and B. A. Bernevig, η -pairing in Hubbard models: From spectrum generating algebras to quantum many-body scars, *Phys. Rev. B* **102**, 085140 (2020).
 - [10] T. Kaneko, T. Shirakawa, S. Sorella, and S. Yunoki, Photoinduced η pairing in the Hubbard model, *Phys. Rev. Lett.* **122**, 077002 (2019).
 - [11] J. Hofmann, M. Krug, N. Ortegel, L. Gérard, M. Weber, W. Rosenfeld, and H. Weinfurter, Heralded entanglement between widely separated atoms, *Science* **337**, 72 (2012).
 - [12] P. Kurpiers *et al.*, Deterministic quantum state transfer and remote entanglement using microwave photons, *Nature* **558**, 264 (2018).
 - [13] P. C. Humphreys, N. Kalb, J. P. J. Morits, R. N. Schouten, R. F. L. Vermeulen, D. J. Twitchen, M. Markham, and R. Hanson, Deterministic delivery of remote entanglement on a quantum network, *Nature* **558**, 268 (2018).
 - [14] P. Barmettler, A. M. Rey, E. Demler, M. D. Lukin,

- I. Bloch, and V. Gritsev, Quantum many-body dynamics of coupled double-well superlattices, *Phys. Rev. A* **78**, 012330 (2008).
- [15] G. J. Mooney, G. A. L. White, C. D. Hill, and L. C. L. Hollenberg, Whole-device entanglement in a 65-qubit superconducting quantum computer, *Adv. Quantum Technol.* **4**, 2100061 (2021).
- [16] D. Bluvstein *et al.*, A quantum processor based on coherent transport of entangled atom arrays, [arXiv:2112.03923](https://arxiv.org/abs/2112.03923) (2021).
- [17] V. Kendon, K. Nemoto, and W. Munro, Typical entanglement in multiple-qubit systems, *J. Mod. Opt.* **49**, 1709 (2002).
- [18] X. Wang, A. Bayat, S. G. Schirmer, and S. Bose, Robust entanglement in antiferromagnetic Heisenberg chains by single-spin optimal control, *Phys. Rev. A* **81**, 032312 (2010).
- [19] I. Sainz, G. Burlak, and A. B. Klimov, Entanglement generation in a spin chain by a pulsed magnetic field: analytical treatment, *Eur. Phys. J. D* **65**, 627 (2011).
- [20] A. Bayat, S. Bose, and P. Sodano, Entanglement routers using macroscopic singlets, *Phys. Rev. Lett.* **105**, 187204 (2010).
- [21] M. P. Estarellas, I. D'Amico, and T. P. Spiller, Robust quantum entanglement generation and generation-plus-storage protocols with spin chains, *Phys. Rev. A* **95**, 042335 (2017).
- [22] I. Pitsios *et al.*, Photonic simulation of entanglement growth and engineering after a spin chain quench, *Nat. Commun.* **8**, 1 (2017).
- [23] D. J. Gross, The role of symmetry in fundamental physics, *Proc. Natl. Acad. Sci.* **93**, 14256 (1996).
- [24] G. Vitagliano, A. Riera, and J. I. Latorre, Volume-law scaling for the entanglement entropy in spin-1/2 chains, *New J. Phys.* **12**, 113049 (2010).
- [25] G. Ramírez, J. Rodríguez-Laguna, and G. Sierra, From conformal to volume law for the entanglement entropy in exponentially deformed critical spin 1/2 chains, *J. Stat. Mech.* **2014**, P10004 (2014).
- [26] H. J. Briegel and R. Raussendorf, Persistent entanglement in arrays of interacting particles, *Phys. Rev. Lett.* **86**, 910 (2001).
- [27] F. H. L. Essler, H. Frahm, F. Göhmann, A. Klümper, and V. E. Korepin, *The One-Dimensional Hubbard Model* (Cambridge University Press, Cambridge, UK, 2005).
- [28] T. Fukuhara *et al.*, Quantum dynamics of a mobile spin impurity, *Nat. Phys.* **9**, 235 (2013).
- [29] W. K. Wootters, Entanglement of formation of an arbitrary state of two qubits, *Phys. Rev. Lett.* **80**, 2245 (1998).
- [30] N. Khaneja, T. Reiss, C. Kehlet, T. Schulte-Herbrüggen, and S. J. Glaser, Optimal control of coupled spin dynamics: design of NMR pulse sequences by gradient ascent algorithms, *J. Magn. Res.* **172**, 296 (2005).
- [31] J.-S. Li, J. Ruths, T.-Y. Yu, H. Arthanari, and G. Wagner, Optimal pulse design in quantum control: A unified computational method, *Proc Natl. Acad. Sci.* **108**, 1879 (2011).
- [32] C. Gross and I. Bloch, Quantum simulations with ultracold atoms in optical lattices, *Science* **357**, 995 (2017).
- [33] A. Blais, A. L. Grimsmo, S. M. Girvin, and A. Wallraff, Circuit quantum electrodynamics, *Rev. Mod. Phys.* **93**, 025005 (2021).
- [34] A. Browaeys and T. Lahaye, Many-body physics with individually controlled Rydberg atoms, *Nat. Phys.* **16**, 132 (2020).
- [35] L.-M. Duan, E. Demler, and M. D. Lukin, Controlling spin exchange interactions of ultracold atoms in optical lattices, *Phys. Rev. Lett.* **91**, 090402 (2003).
- [36] P. N. Jepsen, J. Amato-Grill, I. Dimitrova, W. W. Ho, E. Demler, and W. Ketterle, Spin transport in a tunable Heisenberg model realized with ultracold atoms, *Nature* **588**, 403 (2020).
- [37] R. Ma, B. Saxberg, C. Owens, N. Leung, Y. Lu, J. Simon, and D. I. Schuster, A dissipatively stabilized Mott insulator of photons, *Nature* **566**, 51 (2019).
- [38] C. Monroe *et al.*, Programmable quantum simulations of spin systems with trapped ions, *Rev. Mod. Phys.* **93**, 025001 (2021).
- [39] A. Kantian, A. J. Daley, and P. Zoller, η condensate of fermionic atom pairs via adiabatic state preparation, *Phys. Rev. Lett.* **104**, 240406 (2010).
- [40] B. Kraus, H. P. Büchler, S. Diehl, A. Kantian, A. Micheli, and P. Zoller, Preparation of entangled states by quantum Markov processes, *Phys. Rev. A* **78**, 042307 (2008).
- [41] X. Z. Zhang and Z. Song, Dynamical preparation of a steady off-diagonal long-range order state in the Hubbard model with a local non-Hermitian impurity, *Phys. Rev. B* **102**, 174303 (2020).
- [42] N. Goldman, G. Juzeliūnas, P. Öhberg, and I. B. Spielman, Light-induced gauge fields for ultracold atoms, *Rep. Prog. Phys.* **77**, 126401 (2014).
- [43] A. Eckardt, Colloquium: Atomic quantum gases in periodically driven optical lattices, *Rev. Mod. Phys.* **89**, 011004 (2017).
- [44] M. Boll, T. A. Hilker, G. Salomon, A. Omran, J. Nespolo, L. Pollet, I. Bloch, and C. Gross, Spin- and density-resolved microscopy of antiferromagnetic correlations in Fermi-Hubbard chains, *Science* **353**, 1257 (2016).
- [45] C. A. Regal, M. Greiner, and D. S. Jin, Observation of resonance condensation of fermionic atom pairs, *Phys. Rev. Lett.* **92**, 040403 (2004).
- [46] M. Aidelsburger, M. Atala, M. Lohse, J. T. Barreiro, B. Paredes, and I. Bloch, Realization of the Hofstadter Hamiltonian with ultracold atoms in optical lattices, *Phys. Rev. Lett.* **111**, 185301 (2013).
- [47] M. Nakagawa, N. Tsuji, N. Kawakami, and M. Ueda, η pairing of light-emitting fermions: Nonequilibrium pairing mechanism at high temperatures, [arXiv:2103.13624](https://arxiv.org/abs/2103.13624) (2021).
- [48] J. Tindall, B. Buča, J. R. Coulthard, and D. Jaksch, Heating-induced long-range η pairing in the Hubbard model, *Phys. Rev. Lett.* **123**, 030603 (2019).
- [49] C. Weitenberg and J. Simonet, Tailoring quantum gases by Floquet engineering, *Nat. Phys.* **17**, 1342 (2021).
- [50] M. Müller, S. Diehl, G. Pupillo, and P. Zoller, Engineered open systems and quantum simulations with atoms and ions, *Adv. At. Mol. Opt. Phys.* **61**, 1 (2012).
- [51] T. Shi, E. Demler, and J. I. Cirac, Variational study of fermionic and bosonic systems with non-Gaussian states: Theory and applications, *Ann. Phys.* **390**, 245 (2018).
- [52] M. Kormos, Inhomogeneous quenches in the transverse field Ising chain: scaling and front dynamics, *SciPost Phys.* **3**, 020 (2017).
- [53] W. Magnus, On the exponential solution of differential equations for a linear operator, *Commun. Pure Appl. Math.* **7**, 649 (1954).

[54] H. J. Carmichael, *Statistical Methods in Quantum Optics 1: Master Equations and Fokker-Planck Equations* (Springer, 1999)

Methods

Equation of motion for the qubit array. Our protocol for generating Bell pairs leads to a closed evolution of the two-point correlations $\langle \hat{f}_i^\dagger \hat{f}_j \rangle$ and $\langle \hat{f}_i \hat{f}_j \rangle$, where \hat{f}_i are the JW fermions. In between pulses, they evolve under the free-fermion Hamiltonian, which gives

$$\partial_t \langle \hat{f}_i^\dagger \hat{f}_j \rangle = (iJ/2) \langle \hat{f}_i^\dagger \hat{f}_{j+1} + \hat{f}_i^\dagger \hat{f}_{j-1} - \hat{f}_{i+1}^\dagger \hat{f}_j - \hat{f}_{i-1}^\dagger \hat{f}_j \rangle, \quad (4a)$$

$$\partial_t \langle \hat{f}_i \hat{f}_j \rangle = (iJ/2) \langle \hat{f}_i \hat{f}_{j+1} + \hat{f}_i \hat{f}_{j-1} + \hat{f}_{i+1} \hat{f}_j + \hat{f}_{i-1} \hat{f}_j \rangle \quad (4b)$$

$\forall i, j$, with $\hat{f}_{l+1} := \hat{f}_{l-1} := 0$. A fermionic pulse $\hat{f}_0 + \hat{f}_0^\dagger$ changes the expectation $\langle \hat{O} \rangle$ to $\langle (\hat{f}_0^\dagger + \hat{f}_0) \hat{O} (\hat{f}_0 + \hat{f}_0^\dagger) \rangle$, which couples $\langle \hat{f}_i^\dagger \hat{f}_j \rangle$ and $\langle \hat{f}_i \hat{f}_j \rangle$ through the substitutions

$$\langle \hat{f}_0^\dagger \hat{f}_0 \rangle \longrightarrow 1 - \langle \hat{f}_0^\dagger \hat{f}_0 \rangle, \quad (5a)$$

$$\langle \hat{f}_i^\dagger \hat{f}_0 \rangle \longleftrightarrow \langle \hat{f}_i \hat{f}_0 \rangle^* \quad \forall i \neq 0, \quad (5b)$$

$$\langle \hat{f}_0^\dagger \hat{f}_i \rangle \longleftrightarrow -\langle \hat{f}_0 \hat{f}_i \rangle \quad \forall i \neq 0. \quad (5c)$$

Such a pulse is applied when $\langle \hat{\sigma}_0^z \rangle$ reaches a minimum below 0. This can be monitored using $\hat{\sigma}_0^z = 2\hat{f}_0^\dagger \hat{f}_0 - 1$, which yields

$$\partial_t \langle \hat{\sigma}_0^z \rangle = 2J \text{Im} \langle \hat{f}_{-1}^\dagger \hat{f}_0 - \hat{f}_0^\dagger \hat{f}_1 \rangle, \quad (6a)$$

$$\begin{aligned} \partial_t^2 \langle \hat{\sigma}_0^z \rangle = J^2 \text{Re} \langle \hat{f}_{-1}^\dagger \hat{f}_{-1} + \hat{f}_1^\dagger \hat{f}_1 - 2\hat{f}_0^\dagger \hat{f}_0 \\ + 2\hat{f}_{-1}^\dagger \hat{f}_1 - \hat{f}_{-2}^\dagger \hat{f}_0 - \hat{f}_0^\dagger \hat{f}_2 \rangle, \end{aligned} \quad (6b)$$

where Re and Im denote real and imaginary parts. Therefore, starting with a single \uparrow spin at $i = 0$, we evolve Eqs. (4a) and (4b), making the changes in Eqs. (5a)–(5c) whenever $\partial_t \langle \hat{\sigma}_0^z \rangle = 0$, $\partial_t^2 \langle \hat{\sigma}_0^z \rangle > 0$, and $\langle \hat{\sigma}_0^z \rangle < 0$, for up to l times, as shown in Fig. 2(a) and Extended Data Fig. 2(a).

Spin-spin correlations. The Bell pairs can be detected in experiments by measuring the spin-spin correlations $\langle \hat{\sigma}_i^\nu \hat{\sigma}_j^\nu \rangle$ for $\nu = x, y, z$, plotted in Extended Data Fig. 1. Since the dynamics are generated by a quadratic Hamiltonian, the many-body state is Gaussian [51] and we can find $\langle \hat{\sigma}_i^\nu \hat{\sigma}_j^\nu \rangle$ from $\langle \hat{f}_i^\dagger \hat{f}_j \rangle$ and $\langle \hat{f}_i \hat{f}_j \rangle$ using Wick's theorem. To this end, we first define $\hat{A}_i := \hat{f}_i^\dagger + \hat{f}_i$ and $\hat{B}_i := \hat{f}_i^\dagger - \hat{f}_i$. Substituting $\hat{\sigma}_i^z = \hat{B}_i \hat{A}_i$ in the JW transformation gives, for $i < j$,

$$\langle \hat{\sigma}_i^z \hat{\sigma}_j^z \rangle = \langle \hat{B}_i \hat{A}_i \hat{B}_j \hat{A}_j \rangle, \quad (7a)$$

$$\langle \hat{\sigma}_i^x \hat{\sigma}_j^x \rangle = \left\langle \prod_{k=i}^{j-1} \hat{B}_k \hat{A}_{k+1} \right\rangle, \quad (7b)$$

$$\langle \hat{\sigma}_i^y \hat{\sigma}_j^y \rangle = (-1)^{j-i} \left\langle \prod_{k=i}^{j-1} \hat{A}_k \hat{B}_{k+1} \right\rangle. \quad (7c)$$

Applying Wick's theorem to Eq. (7a), we find

$$\langle \hat{\sigma}_i^z \hat{\sigma}_j^z \rangle = \langle \hat{B}_i \hat{A}_i \rangle \langle \hat{B}_j \hat{A}_j \rangle - \langle \hat{B}_i \hat{B}_j \rangle \langle \hat{A}_i \hat{A}_j \rangle + \langle \hat{B}_i \hat{A}_j \rangle \langle \hat{A}_i \hat{B}_j \rangle. \quad (8)$$

Similarly, the string correlation in $\langle \hat{\sigma}_i^x \hat{\sigma}_j^x \rangle$ [Eq. (7b)] can be reduced to the Pfaffian of an antisymmetric matrix $\mathbf{\Gamma}^x$ [52] of size $2(j-i)$, with the elements

$$\mathbf{\Gamma}_{m,n}^x = \begin{pmatrix} \langle \hat{B}_m \hat{B}_n \rangle + \delta_{m,n} & \langle \hat{B}_m \hat{A}_{n+1} \rangle \\ \langle \hat{A}_{m+1} \hat{B}_n \rangle & \langle \hat{A}_{m+1} \hat{A}_{n+1} \rangle - \delta_{m,n} \end{pmatrix} \quad (9)$$

where $m, n = i, i+1, \dots, j-1$. One can find $\mathbf{\Gamma}_{m,n}^x$ using

$$\langle \hat{A}_m \hat{A}_n \rangle = \delta_{m,n} + 2i \text{Im} \langle \hat{f}_m \hat{f}_n + \hat{f}_m^\dagger \hat{f}_n \rangle, \quad (10a)$$

$$\langle \hat{B}_m \hat{B}_n \rangle = -\delta_{m,n} + 2i \text{Im} \langle \hat{f}_m \hat{f}_n - \hat{f}_m^\dagger \hat{f}_n \rangle, \quad (10b)$$

$$\langle \hat{A}_m \hat{B}_n \rangle = \delta_{m,n} - 2i \text{Re} \langle \hat{f}_m \hat{f}_n + \hat{f}_m^\dagger \hat{f}_n \rangle, \quad (10c)$$

$$\langle \hat{B}_m \hat{A}_n \rangle = -\langle \hat{A}_n \hat{B}_m \rangle. \quad (10d)$$

From Eq. (7c), $\langle \hat{\sigma}_i^y \hat{\sigma}_j^y \rangle$ can be obtained by interchanging \hat{A} and \hat{B} in $\mathbf{\Gamma}^x$ and multiplying the resulting Pfaffian by $(-1)^{j-i}$.

Robustness for Hamiltonian perturbations. In the presence of a perturbation $\epsilon \hat{H}'$, the dynamics are generated by $\hat{U}(t) = e^{-i(\hat{H} + \epsilon \hat{H}')t}$. Using the Zassenhaus formula [53], we write

$$\hat{U}^\dagger(t) = e^{i\hat{H}t} [1 - \epsilon \hat{P}(t) + \mathcal{O}(\epsilon^2)], \quad (11)$$

where $\hat{P}(t)$ is an anti-hermitian operator given by

$$\hat{P}(t) = \sum_{n=1}^{\infty} \frac{(-it)^n}{n!} [(\hat{H})^{n-1}, \hat{H}'], \quad (12)$$

$$\text{with } [(\hat{H})^n, \hat{H}'] := \underbrace{[\hat{H}, \dots, [\hat{H}, \hat{H}']]}_{n \text{ times}}, \quad (13)$$

and $[(\hat{H})^0, \hat{H}'] := \hat{H}'$. Hence, the change in the expectation value of an operator \hat{O} at time t is

$$\begin{aligned} \delta \langle \hat{O} \rangle(t) &= \langle \Psi(0) | \hat{U}^\dagger(t) \hat{O} \hat{U}(t) - e^{i\hat{H}t} \hat{O} e^{-i\hat{H}t} | \Psi(0) \rangle \\ &= \epsilon \langle \Psi(t) | [\hat{O}, \hat{P}(t)] | \Psi(t) \rangle + \mathcal{O}(\epsilon^2), \end{aligned} \quad (14)$$

where $|\Psi(t)\rangle$ is the state of the unperturbed system. So, the first-order correction vanishes provided $\langle [\hat{O}, \hat{P}(t)] \rangle = 0$. From Eq. (12), this is true at all times if $\langle [\hat{O}, [(\hat{H})^n, \hat{H}']] \rangle = 0 \forall n$. This condition is, in fact, satisfied for the operators \hat{C} and $\hat{\sigma}_0^z$ for a number of common perturbations \hat{H}' , leading to the quadratic variations in Fig. 3.

Equation of motion with perturbations. The dynamics remain free fermionic for a number of variations, including nonuniform coupling J_i , Zeeman splittings ϵ_i , and dephasing rates $\gamma_i > 0$. The first two are described by the Hamiltonian

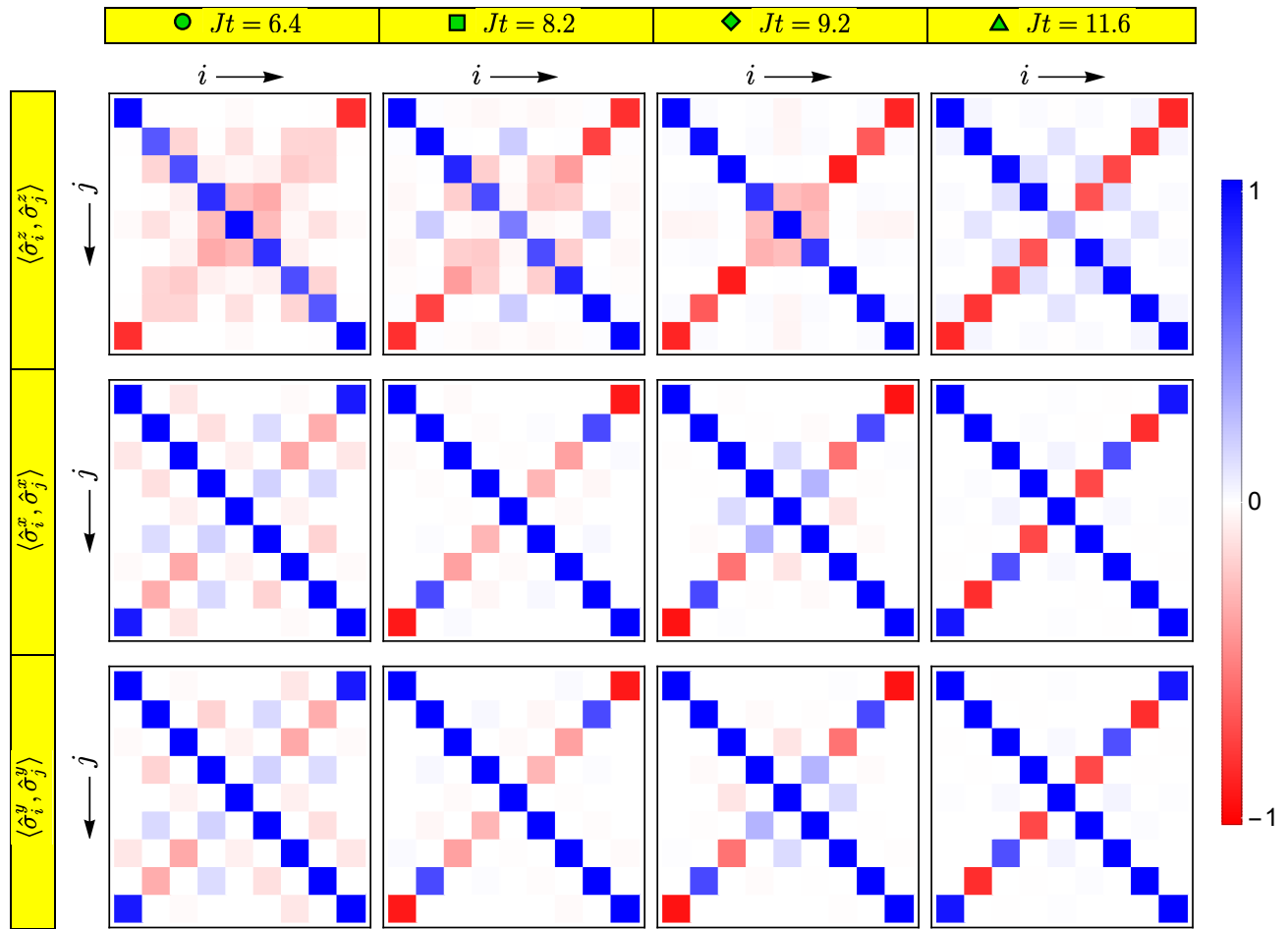
$$\hat{H} = -\frac{1}{2} \sum_{i=-l}^{l-1} (J_i \hat{f}_i^\dagger \hat{f}_{i+1} + \text{h.c.}) + \sum_{i=-l}^l \epsilon_i \hat{f}_i^\dagger \hat{f}_i, \quad (15)$$

whereas the dephasing can be modeled by Lindblad operators $\hat{L}_i = \sqrt{\gamma_i} \hat{\sigma}_i^z / 2$ under a standard Born-Markov approximation [54], resulting in the evolution

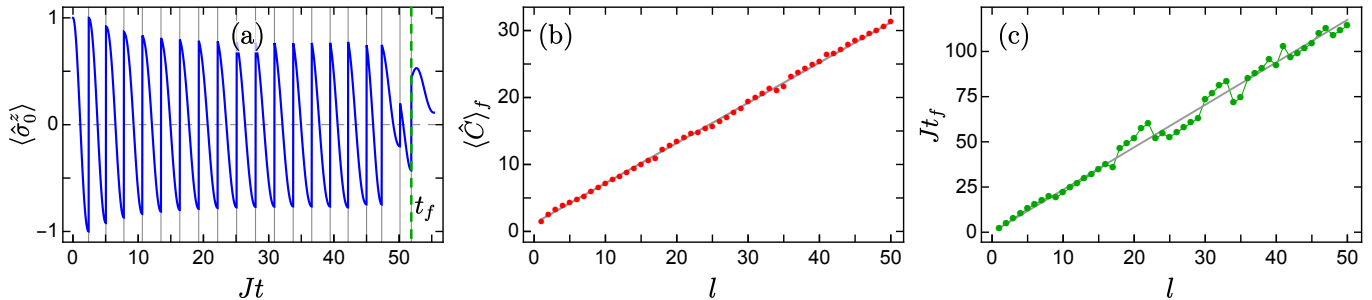
$$\partial_t \langle \hat{O} \rangle = i \langle [\hat{H}, \hat{O}] \rangle + \sum_i \langle [\hat{L}_i, [\hat{O}, \hat{L}_i]] \rangle \quad (16)$$

for any hermitian operator \hat{O} . The dephasing causes local coherences to decay at a rate γ_i , i.e., $\partial_t \langle \hat{\sigma}_i^x \rangle_L = -\gamma_i \langle \hat{\sigma}_i^x \rangle$, where the subscript L denotes the dephasing component. The correlations $\langle \hat{f}_i^\dagger \hat{f}_j \rangle$ and $\langle \hat{f}_i \hat{f}_j \rangle$ again form a closed set of equations, which can be found from Eq. (16) by straightforward algebra.

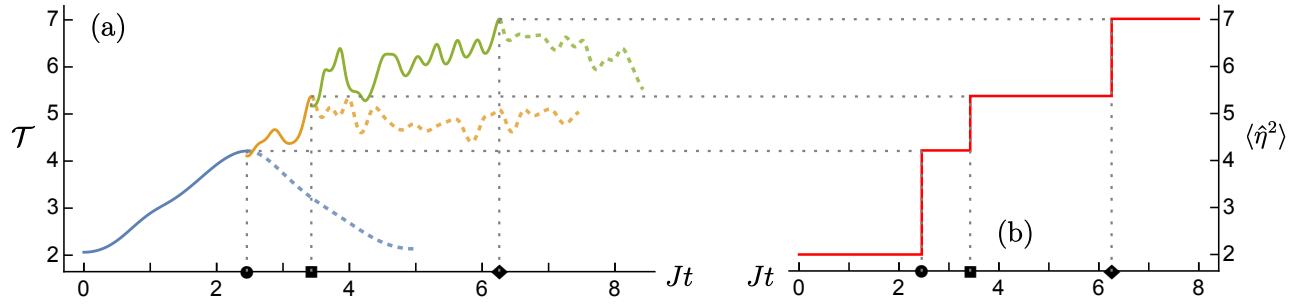
Similarly, one can include an XY anisotropy, which adds pairing terms $\hat{f}_i \hat{f}_j$ to the Hamiltonian. For other perturbations such as a z - z coupling, long-range interactions, or incoherent spin flips, the system is no longer free fermionic and we perform a full many-body simulation.



Extended Data Fig. 1. **Spin-spin correlations.** Time evolution of $\langle \hat{\sigma}_i^\nu, \hat{\sigma}_j^\nu \rangle := \langle \hat{\sigma}_i^\nu \hat{\sigma}_j^\nu \rangle - \langle \hat{\sigma}_i^\nu \rangle \langle \hat{\sigma}_j^\nu \rangle$ for a 9-site XX chain from exact diagonalization, reflecting the successive stacking of Bell pairs between mirror-conjugate sites in Figs. 2(c-f). Pulses are applied at times $Jt = 2.4, 5.0, 7.8, 10.2$, when the phase correlations $\langle \hat{\sigma}_i^x, \hat{\sigma}_{-i}^x \rangle$ and $\langle \hat{\sigma}_i^y, \hat{\sigma}_{-i}^y \rangle$ flip sign. Note that $\langle \hat{\sigma}_i^x \rangle = \langle \hat{\sigma}_i^y \rangle = 0$.



Extended Data Fig. 2. **Finite-size scaling.** (a) Evolution of the center-spin magnetization, $\langle \hat{\sigma}_0^z \rangle$, during our protocol for 47 sites ($l = 23$) from exact diagonalization. The last pulse is applied at time t_f , after which $\langle \hat{\sigma}_0^z \rangle$ reaches a minimum above 0; continuing beyond this point does not yield significant gains. (b) Final value of $\langle \hat{C} \rangle_f$ as a function of l , compared with $0.6(l+2)$ shown by the gray line. Note that $\langle \hat{C} \rangle$ is bounded by $l+1/2$. (c) Duration as a function of l ; gray line shows $2.35l$. The sudden small fluctuations are due to variation in the number of pulses, which fluctuates around $0.8l$ for large l .



Extended Data Fig. 3. **Illustration of the protocol for generating η pairs.** Evolution of a Fermi-Hubbard chain with 8 sites and $U/J = 10$ using exact diagonalization. (a) Efficacy $\mathcal{T} := \langle \hat{\mathcal{J}} \hat{\eta}^2 \hat{\mathcal{J}} \rangle / \langle \hat{\mathcal{J}}^2 \rangle$ is monitored for a duration $U/(2J^2)$ and the next pulse of $\hat{\mathcal{J}}$ is applied when \mathcal{T} is maximum, shown by the dotted vertical lines. Solid curves show the resulting piecewise evolution. (b) $\langle \hat{\eta}^2 \rangle$ is conserved in between pulses and jumps to the instantaneous value of \mathcal{T} after the application of each pulse.